ADVANCED MATERIALS INTERFACES
Open Access
www.advmatinterfaces.de

Solar Cells on Multicrystalline Silicon Thin Films Converted from Low-Cost Soda-Lime Glass

Ingrid Schall, Guobin Jia, Uwe Brückner, Annett Gawlik, Christian Strelow, Jan Krügener, Ditian Tan, Michael Fahrbach, Stefan G. Ebbinghaus, Jonathan Plentz, and Erwin Peiner**

Fabrication and characterization of solar cells based on multicrystalline silicon (mc-Si) thin films are described and synthesized from low-cost soda-lime glass (SLG). The aluminothermic redox reaction of the silicon oxide in SLG during low-temperature annealing at 600 – 650 °C leads to an mc-Si thin film with large grains of lateral dimensions in the millimeter range, and moderate *p*-type conductivity with an average Al acceptor concentration between 5×10^{16} and 1.2×10^{17} cm^{-3} in the bulk. A residual composite layer of mainly alumina and unreacted Al forms beneath the mc-Si thin film as the second product of the crystalline silicon synthesis (CSS) process, which can be used as rear contact in a vertical solar cell design. The mc-Si absorber (≈10 µm) is thin enough that the diffusion length given by a minority carrier lifetime of ≈1 µs exceeds the path length to the top contact several times. Homojunction and heterojunction diodes have been fabricated on the mc-Si thin films and show great potential of CSS for the realization of high-performance solar cells.

1. Introduction

Crystalline silicon is needed in large and ever-increasing amounts, in particular for photovoltaic (PV) energy conversion. Efficient thin-film absorbers, for example, based on abundant and stable compound semiconductors, were considered to reduce material consumption. Recently, solar cells in Sb_2Se_3 or Cu_2CdSnS_4 with 350 and 522-nm-thick absorbers on soda lime glass (SLG) yielded power conversion efficiencies of 2.41% and 10.1%, respectively.[1,2] In the case of Sb_2Se_3, which was produced without toxic elements like Cd, PV performance is still rather low, but was expected to improve by increasing absorber thickness and reducing trap-assisted carrier recombination.[1]

Alternatively, thin-film multicrystalline (mc) silicon on glass can help to save both energy and material consumption compared to full-silicon-wafer technologies. Competitive PV conversion efficiencies can be expected on thin-film silicon absorbers (10 – 15 µm) using a photonic-crystal light-trapping structure.[3] Fabrication approaches for thin-film mc-Si on glass mostly used liquid phase crystallization (LPC), in which electron-beam-evaporated amorphous/nanocrystalline silicon (a-/nc-Si) on technical glass such as aluminosilicate glass was subsequently melted by a scanning laser beam.[4,5] Solar cells fabricated with LPC mc-Si showed maximum power conversion efficiencies of 15.1% and 15.8% respectively.[6,7] Due to the absence of a rear-contact layer on the glass, only one-side-contact designs were feasible. Furthermore, an efficiency of only 4.3% was achieved, when the technical glass substrate was replaced by much cheaper and abundant SLG.[8] In this case, spalling of the LPC absorbers from the substrate was observed, limiting the absorber thickness to 6 µm, which is too small for efficient light-capture. Stress-induced during the solidification of the molten Si from 1410 °C to room

I. Schall
sameday media GmbH
Am Flatthaus 13, 29640 Schneverdingen, Germany

G. Jia, U. Brückner, A. Gawlik, J. Plentz
Department Functional Interfaces
Leibniz Institute of Photonic Technology (Leibniz IPHT)
Albert-Einstein-Str. 9, 07745 Jena, Germany
E-mail: jonathan.plentz@leibniz-ipht.de

The ORCID identification number(s) for the author(s) of this article can be found under https://doi.org/10.1002/admi.202400170

© 2024 The Author(s). Advanced Materials Interfaces published by Wiley-VCH GmbH. This is an open access article under the terms of the Creative Commons Attribution License, which permits use, distribution and reproduction in any medium, provided the original work is properly cited.

DOI: 10.1002/admi.202400170

C. Strelow
Institut für Physikalische Chemie
Universität Hamburg
Grindelallee 117, 20146 Hamburg, Germany

J. Krügener
Institut für Materialien und Bauelemente der Elektronik (MBE)
Leibniz Universität Hannover
Schneiderberg 32, 30167 Hannover, Germany

D. Tan, M. Fahrbach, E. Peiner
Institut für Halbleitertechnik / Laboratory for Emerging Nanometrology (LENA)
Technische Universität Braunschweig
Hans-Sommer-Str. 66, 38106 Braunschweig, Germany
E-mail: e.peiner@tu-braunschweig.de

S. G. Ebbinghaus
Institut für Chemie
Martin-Luther-Universität Halle-Wittenberg
Kurt-Mothes-Str. 2, 06120 Halle, Germany

temperature under the large mismatch of thermal expansion coefficients of silicon and SLG was identified as a primary cause of the detrimental failure.[8]

An entirely different approach for PV on SLG, which involves extracting the PV absorber from the glass rather than depositing or melting onto its surface, is the recently reported crystalline silicon synthesis (CSS) process.[9,10] CSS is based on the aluminothermic redox reaction of silicon dioxide in SLG, which produces silicon leaving alumina behind:

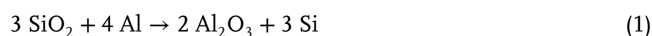

$$3\ SiO_2 + 4\ Al \rightarrow 2\ Al_2O_3 + 3\ Si \tag{1}$$

During the CSS process crystalline silicon grows laterally with millimeter-sized grains, which until now, is only known for crystallization from the melt. A mc-Si/Al_2O_3:Al/SLG layer stack is generated, in which unprocessed aluminum is incorporated in the alumina and thus available for a rear contact on the SLG for electronic devices with vertical architecture.

In comparison with full-silicon-wafer processing, CSS consumes much less energy, that is, only for producing the source materials SLG (4-mm-thick) and Al (20-µm-thick) and to a much lower extent for the aluminothermic-synthesis process itself. Estimation yields a value per wafer area of ≈ 37 kW h m^{-2} for CSS mc-Si, that is, much less than 160-µm-thick full-wafer mc-silicon, which requires electricity per area of ≈ 100 to 140 kW h m^{-2} (see Supporting Information).

At first glance, the silicon crystallization of the CSS process appears to be similar to the well-known aluminum-induced- crystallization (AIC) process.[11] However, CSS yields larger grain sizes (mm-size vs 250 µm) and lower net carrier concentration ($3 - 5 \times 10^{18}$ cm^{-3} vs $0.5 - 2 \times 10^{19}$ cm^{-3}) than AIC which is processed below the eutectic temperature of Al-Si (577 °C).[7] According to the Al-Si phase diagram at 600–650 °C Al can be dissolved up to an amount of ≈ 1 at. % silicon. At concentrations above, silicon starts to crystallize from the supersaturated solution. Al_2O_3 as the second product of the aluminothermic reaction (Equation 1) replaces the SiO_2 below the original glass surface. Due to its smaller molecular volume compared to SiO_2, the Al_2O_3 contains pores, through which aluminum can be continuously transported to the surface of the SLG, thereby maintaining the aluminothermic reduction of SiO_2 underneath the composite Al_2O_3:Al layer.

Cross-sectional scanning electron microscopy (SEM) and superimposed element mappings by energy-dispersive X-ray fluorescence (EDX) confirmed a sharp interface without voids between the mc-Si layer and the SLG.[10] EDX showed an abrupt transition of the dominating component from silicon (in the mc-Si layer) to aluminum (Al_2O_3 and Al in a $\approx$35-µm-thick layer of the reacted SLG below the mc-Si layer). Oxygen was measured across the reacted (Al_2O_3) and pristine (SiO_2) regions of the SLG. The composite structure of Al_2O_3:Al of the reacted SLG was optically visible (in a grinded dimple) by a dark metallic surface finish, which brightened to the color of alumina after etching in aluminum cleaner (AL 80, UN 3265).

Due to the mismatch in thermal expansion coefficients between Si and SLG, the mc-Si is expected to be under compressive stress, which was measured to ≈ -0.3 to -0.5 GPa.[10] Because of much smaller temperature difference between process and room temperature of $\Delta T \approx -600$ K compared to LPC, CSS is much less affected by thermal stress. Correspondingly, delamination of CSS mc-Si layers from the SLG was not observed. An increase of doping concentration toward its bottom was detected causing a back-surface field (BSF) in the absorber.[10] Furthermore, the Al_2O_3:Al composite layer may be used as an inherent rear contact. Both, BSF and rear contact are beneficial for a vertical full-emitter solar cell design.

In the following, we report on the characterization of mc-Si by CSS on SLG as well as thin-film homojunction and heterojunction solar-cell test structures fabricated with it. The fabrication process of a Heterojunction with Intrinsic Thin Layer (HIT) solar cell is schematically displayed in **Figure 1**. Each step is described in detail in Section 4. Optimization of the mc-Si absorber material is addressed with respect to doping for further improvement of the PV performance.

2. Results and Discussion

To investigate the PV quality of mc-silicon on soda-lime glass fabricated by the CSS process, different designs of solar-cell test structures are possible, which, however have to take into account a specific feature of the CSS material. A thin transparent layer (20 to 50 nm) is formed during CSS (see Figure S1, Supporting Information), which is resistant against standard wet and dry chemical etching treatment, and can be removed only physically by diamond-paste polishing or fs-laser irradiation. The latter method has the advantage that the inert layer can be maskless-removed in selected areas (e. g. for electrical contacts) but remains otherwise as a possible transparent passivation layer. The composition of the inert layer is determined by X-ray photoelectron spectroscopy (XPS, see Figure S2, Supporting Information). We find contributions of alumina (Al_2O_3), silica (SiO_2) and aluminosilicate (Al_2SiO_5) in the layer, an occasionally observed carbon peak (not shown here) is attributed to cracked hydrocarbons from the residual gas in the XPS chamber deposited on the sample. The small silica signatures in Figure S2 (Supporting Information) may originate from sites, with gaps in the inert layer (sidewalls of the silicon grains), where silicon oxide on the mc-Si can be expected. Analyzing the XPS data at four different position of one sample and one position of a second sample we find a composition of Al : Si : O of 31% : 9% : 50% (see Table S1, Supporting Information), which we assign to a mixture of alumina (Al_2O_3) or aluminosilicate (Al_2SiO_5).

PV performance depends on the absorber-material quality, which can be improved, for example, by reducing the absorber doping concentration level measured previously.[10] Low acceptor/net-carrier concentration in the absorber is a prerequisite to decrease Auger recombination, which is the limiting factor of PV performance at high acceptor concentrations. **Figure 2** shows the Al concentration measured by secondary ion mass spectroscopy (SIMS) at two positions in mc-Si synthesized under improved CSS conditions compared to the reference. Nearly constant Al concentrations of $\approx 5 \times 10^{16}$ and $\approx 1.2 \times 10^{17}$ cm^{-3} are determined by SIMS in the bulk. Furthermore, a sharp decrease of the Al concentration to the $\approx 2 \times 10^{16}$ and $\approx 5 \times 10^{16}$ cm^{-3} is observed close to the surface. The concentrations are considerably lower (by a factor of 30 to 60 times in the bulk (and even more at the surface) compared with a previous SIMS measurement (reference CSS mc-Si).[10]

© 2024 The Author(s). Advanced Materials Interfaces published by Wiley-VCH GmbH

RIGHTSLINK Copyright Clearance Center

21967350, 2024, 28, Downloaded from https://onlinelibrary.wiley.com/doi/10.1002/admi.202400170 by Fak-Martin Luther Universitats, Wiley Online Library on [05/11/2024]. See the Terms and Conditions (https://onlinelibrary.wiley.com/terms-and-conditions) on Wiley Online Library for rules of use; OA articles are governed by the applicable Creative Commons License

21967350, 2024, 28, Downloaded from https://onlinelibrary.wiley.com/doi/10.1002/admi.202400170 by Fak-Martin Luther Universitats, Wiley Online Library on [05/11/2024]. See the Terms and Conditions (https://onlinelibrary.wiley.com/terms-and-conditions) on Wiley Online Library for rules of use; OA articles are governed by the applicable Creative Commons License

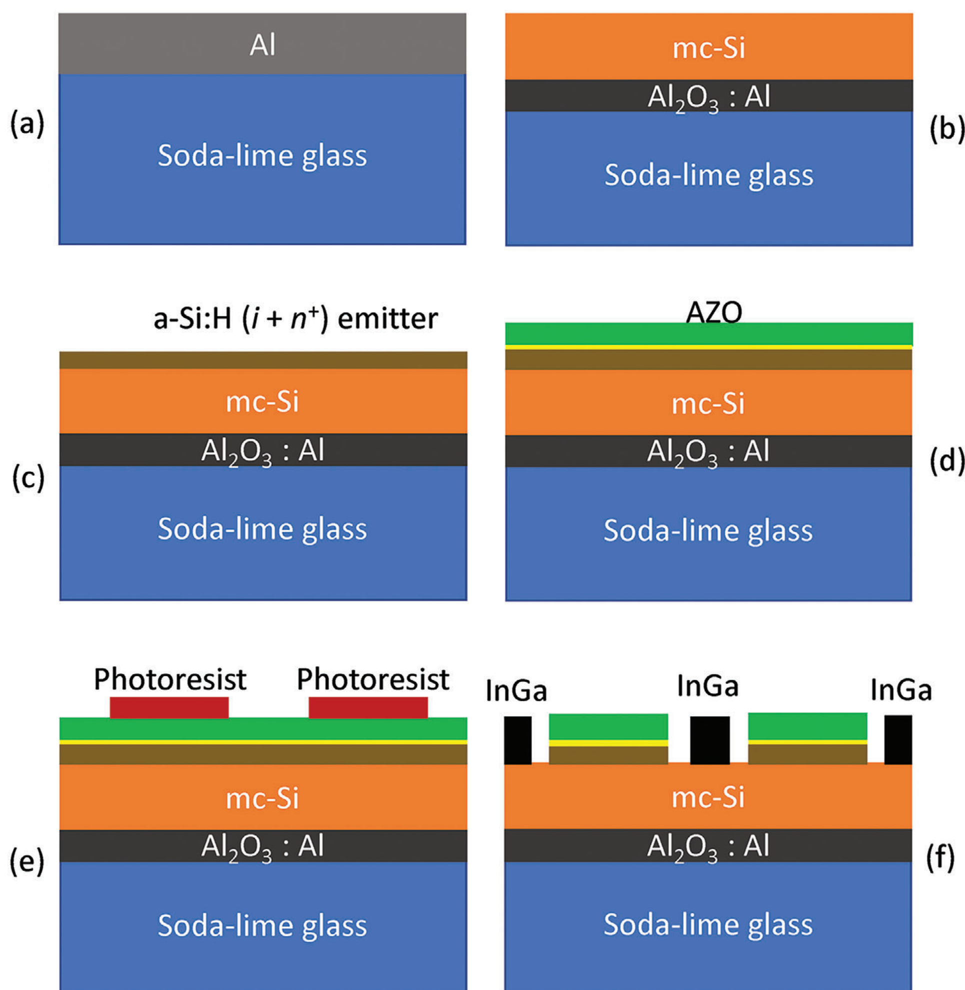

Figure 1. Schematic of the fabrication process of a HIT-emitter solar cell on CSS mc-Si on SLG. a) Al layer deposition, b) aluminothermic reaction followed by surface-finishing steps, c) a-Si:H ($i + n^+$) emitter deposition by plasma-enhanced chemical vapor deposition (PECVD), d) atomic layer deposition (ALD) of an ultrathin Al_2O_3 (1 nm) followed by aluminum-doped ZnO (AZO) for a passivating tunnel contact to the HIT, e) mesa cell structuring, f) rear-contact formation by an InGa alloy. For a detailed description of the fabrication process of a HIT-emitter solar cell on CSS mc-Si, see Section 4.

To confirm these findings, we performed micro Raman spectroscopy measurements revealing a nearly ideal Lorentz-shaped spectral line of the optical phonon mode of CSS mc-Si without a detectable asymmetry, which indicates hole concentrations much lower than 1×10^{18} cm^{-3} (see Figure S4, Supporting Information). Doping concentrations below $\approx 1 \times 10^{18}$ cm^{-3} were not expected regarding the solid solubility of Al in silicon at 600 – 650 °C.[12] This depletion of Al from the mc-Si may be inherent to the CSS process, during which the Al atoms in the mc-Si follow the gradient of the chemical potential toward the glass substrate via the composite Al_2O_3 : Al layer underneath. A low potential is maintained here, induced by the continued consumption of Al for the aluminothermic reduction of SiO_2.

In photoluminescence (PL) measurements on CSS mc-Si we found minority-carrier lifetimes in the 0.6 to 3 µs range using time-correlated single photon counting,[10] which is shorter than expected for Al concentrations $\approx 1 \times 10^{17}$ cm^{-3}.[13,14] Nevertheless, the measured lifetimes are an order of magnitude longer compared to only ≈200 ns for mc-Si thin films of similar donor doping concentration fabricated by LPC on glass.[8,15] The long lifetimes of CSS mc-Si could be a result of large grain size, low concentration of interstitially dissolved impurities (e.g. iron) or an efficient back-surface passivation by the Al_2O_3 : Al composite layer underneath the mc-Si.

As a first solar-cell test structure, a homojunction diode with an n^+-doped emitter was fabricated (see Section S2, Supporting Information). For this, phosphorus implantation followed by dopant activation was done using a low-temperature process to avoid excessive stress and damage to the CSS mc-Si. Both the introduced thermal energy and the induced temperature gradient should be kept as low as possible while ensuring full dopant activation. For this, a plate heater was used at a constant temperature on the glass bottom side combined with a pulsed radiant heater (pulses of seconds duration) positioned at a changeable distance to the CSS mc-Si layer surface.

First, samples underwent a phosphorus implantation at 60 keV and a dose of 1×10^{16} cm^{-2} were investigated to find an optimal dopant activation. Figure S5 (Supporting

© 2024 The Author(s). Advanced Materials Interfaces published by Wiley-VCH GmbH
RIGHTSLINK

21967350, 2024, 28, Downloaded from https://onlinelibrary.wiley.com/doi/10.1002/admi.202400170 by Fak-Martin Luther Universitats, Wiley Online Library on [05/11/2024]. See the Terms and Conditions (https://onlinelibrary.wiley.com/terms-and-conditions) on Wiley Online Library for rules of use; OA articles are governed by the applicable Creative Commons License

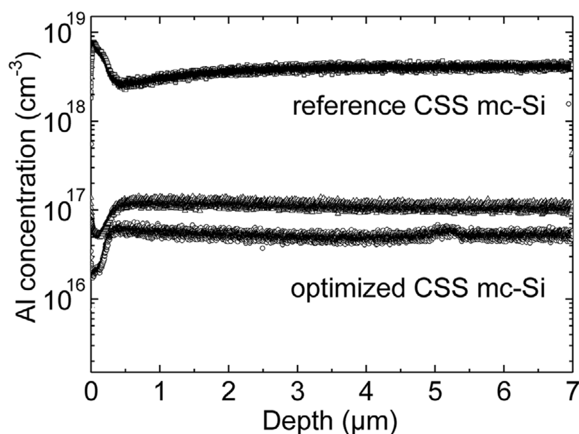

Figure 2. SIMS measurements were carried out on two optimized CSS-Si samples with respect to the previous reference.[10] A nearly constant aluminum concentration of $\approx 5 \times 10^{16}$ and $\approx 1.2 \times 10^{17}$ cm^{-3} is visible over a large depth range of 7 µm, starting from $\approx 2 \times 10^{16}$ and $\approx 5 \times 10^{17}$ cm^{-3}, respectively, at the top of the mc-Si layers.

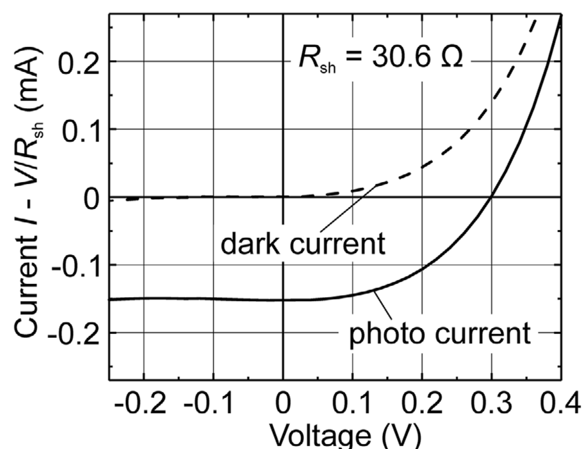

Figure 3. Shunt-resistance-corrected characteristics ($I - V/R_{sh}$ vs V) of a homojunction-type solar cell with implanted/annealed emitter and evaporated Au/Cr emitter and absorber contacts.

Information) shows electrochemical capacitance-voltage (ECV) measurements of implanted mc-Si after thermal treatment. Depending on annealing conditions, fully or partially activated n^+p junctions were obtained, and maximum electron concentrations $\approx 6 \times 10^{20}$ cm^{-3} were achieved. Junction depths of 170 to 180 nm were determined. However, formation of local-spalling defects in the mc-Si layer of 10^{-2} to 10^{-1} µm in diameter was observed, occurring at long IR pulse duration and short distance of the lamp to the sample surface. On the other hand, at much shorter pulse duration (5 s) the phosphorus in the mc-Si layer was not fully activated.

To keep the implantation and annealing load to the CSS sample as low as possible, doping was done at a lower dose of 1×10^{15} cm^{-2} in the following. For annealing an SLG backside temperature of 600 °C and a front-side lamp pulse on the mc-Si of 10 s duration at a distance of 11.4 mm were chosen. Photographs of samples after implantation, annealing, and cleaning in buffered HF solution are displayed in Figure S6a,b (Supporting Information), respectively. Before implantation, a part of the sample (for the absorber contact) was masked using adhesive foil. Furthermore, in selected areas the thin aluminum oxide layer was removed by fs-pulse laser ablation, while on the remaining surface it was kept to act as a transparent passivation layer. In the ablated areas an Au (300 nm)/Cr (30 nm) contact metallization was deposited (Figure S6c, Supporting Information) by electron-beam evaporation through a shadow mask to form the emitter and absorber contacts.

I-V curves measured between the *p*- and *n*-contacts under illumination with a Xe halogen lamp showed photocurrents increasing proportional to the illumination intensity. We found a nearly Ohmic characteristic with a short-circuit current of 0.15 mA and an open-circuit voltage of 4.6 mV, corresponding to a shunt resistance of $R_{sh} = 30.6$ Ω. Diode characteristics were observed after subtracting the shunt current, that is, as $I - V/R_{sh}$ versus V (**Figure 3**), and the respective pseudo open circuit voltage amounted to ≈ 0.3 V. We assign the low shunt resistance to the local-spalling defects in the mc-Si layer generated during annealing after implantation. Thereby, the n^+p emitter-absorber junction may have been exposed and short-circuited by the Au/Cr metallization. Furthermore, hole transport may be affected by the alumina in the rear contact layer as reported with electron transport through oxidized Al contacts on Sb_2Se_3-based solar cells.[16]

Therefore, instead of the homojunction-type cell with its necessary temperature treatment to the CSS wafer, we employed the HIT emitter technology combined with a transparent conductive oxide (TCO) contact, which has been extensively investigated before with LPC silicon absorbers on glass.[4,5] Before starting device fabrication, the thin inert layer (Figure S1, Supporting Information), which is created during the CSS process, was removed by diamond-paste polishing. The surface of the mc-Si was etched afterward with potassium hydroxide (KOH) solution. The surface roughness of the mc-Si measured by confocal laser scanning spectroscopy (CLSM) of $Ra = 180 - 250$ nm, was first reduced to $Ra = 60 - 120$ nm after polishing for 90 s with 0.25-µm-diamond paste. After KOH etching it re-increased to $Ra = 0.1 - 0.4$ µm.

The fabrication process of the heterojunction-type solar cell shown in Figure 1 is described in detail in Section 4. Here, special emphasis was put on the influence of a perchloric-acid-based etching prior to the HIT- and TCO-layer deposition, which was done using plasma-enhanced chemical vapor deposition (PECVD) and atomic layer deposition (ALD), respectively, at 225 °C. The top part of the mc-Si layer was etched for 0, 4, and 20 s at an etching rate of ≈15 µm min^{-1} resulting in removed layer thicknesses of 0, 1, and 5 µm (of samples A, B, and C), respectively. The current-density versus voltage (*J*–*V*) characteristics measured at AM 1.5 G are presented in **Figure 4** and the PV parameters determined are summarized in **Table 1**. The active areas of the cells are almost the same, that is, 3.61, 3.70, and 3.69 mm^2 for samples A, B, and C, respectively.

The cells fabricated on the substrate, which was not etched by perchloric-acid-based solution, show very poor PV parameters, with open circuit voltage (V_{OC}) of 63 mV, short-circuit current density (J_{SC}) of 2.92 mA cm^{-2}, fill factor (*FF*) of 25.0%, and conversion efficiency of only 0.05%. The cell is affected by a specific shunt (ρ_{sh}) and series resistivity (ρ_s) of 22 and 20 Ω cm^2,

© 2024 The Author(s). Advanced Materials Interfaces published by Wiley-VCH GmbH
RIGHTSLINK

21967350, 2024, 28, Downloaded from https://onlinelibrary.wiley.com/doi/10.1002/admi.202400170 by Fak-Martin Luther Universitats, Wiley Online Library on [05/11/2024]. See the Terms and Conditions (https://onlinelibrary.wiley.com/terms-and-conditions) on Wiley Online Library for rules of use; OA articles are governed by the applicable Creative Commons License

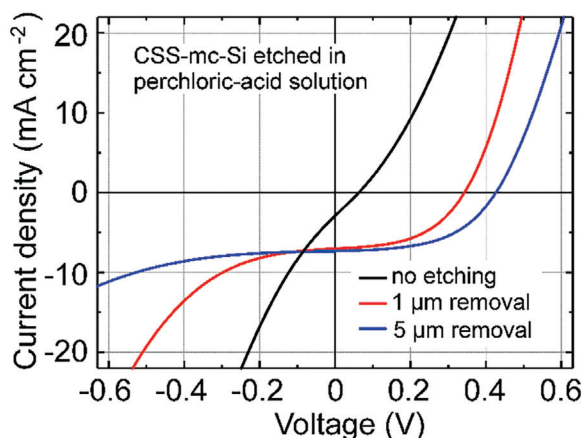

Figure 4. Current-density versus voltage (*J*–*V*) characteristics of mesa-type solar cells with HIT emitter and AZO as TCO emitter contact measured at AM 1.5 G illumination. The black line presents the *J*–*V* characteristic of an un-etched sample (A), the red line is for a sample after 1-μm-top-layer removal (B), and the blue line is for a sample after 5-μm-top-layer removal (C).

respectively. The large surface roughness after KOH etching, which may have caused not perfectly conformal coverage of the mc-Si absorber by the very thin HIT emitter layers, or a defect-rich damage layer at the surface of the mc-Si[10] was assumed as the origin of the shunt current.

A 1-μm top-layer removal by the perchloric-acid solution etching improves significantly the PV performance, solar cells with V_{OC} of 343 mV, J_{SC} of 7.00 mAcm,$^{-2}$ FF of 49.4%, and a conversion efficiency of 1.18% were reached. The ρ_{sh} is improved by more than one order of magnitude to 408 Ω cm^2, and the ρ_s is significantly reduced to 13 Ω cm^2.

A 5-μm top-layer removal further increases the open-circuit voltage to V_{OC} of 426 mV, while the short-circuit current shows a slight improvement to J_{SC} of 7.32 mA cm^{-2}. Correspondingly, fill factor and conversion efficiency increases moderately to 52.3% and 1.63%, respectively. This is in line with a value of ρ_{sh} doubled to 964 Ω cm^2, while ρ_s of 14 Ω cm^2 remained almost unchanged. An early breakdown of the cells at reverse bias was observed for all the three samples. The unetched samples showed a breakdown at −0.1 V. This value improved with the duration of the perchloric-acid solution etching from −0.2 to −0.4 V for samples B and C, respectively.

The measured characteristics indicate that the treatment of the mc-Si in perchloric-acid solution improves the PV performance of heterojunction-type solar cells. Due to its isotropic behavior surface roughness has been reduced for better conformal coverage of the mc-Si absorber by the very thin HIT emitter layers. Residual polishing damage of the mc-Si as a further cause of the early breakdown at reverse bias conditions has been removed by the etching in perchloric-acid solution.

Unfortunately, the perchloric-acid etching reduces the active mc-Si thickness as well, only ≈2.6 μm-thick absorber is left on the sample C. The loss of the active mc-Si may explain the rather low J_{SC} reached on samples B and C. An ideal etchant should selectively remove only the defective regions without loss of active mc-Si material. Nevertheless, the measured PV parameters on etched mc-Si are much better than those without etching in perchloric-acid solution and represent the first proof of solar-cell-grade mc-Si using CSS.

In the case of the solar cells in Figure 4 and Table 1, both electrodes are prepared on the front side, with no current flow expected through the bottom alumina/aluminum composite layer. The p^+/p back surface field provided in the transition region between the mc-Si and the alumina/aluminum composite layer can be of additional benefit here. Therefore, an unfavorable effect of the alumina on carrier transport[16] is not expected here.

The process parameters of CSS and measured PV parameters are collected in Table S2 (Supporting Information). Compared with the results reported for an LPC absorber on SLG, we find a worse PV performance for CSS mc-Si except for the fill factor, which we relate to absorber thickness, doping concentration, and carrier type. Lower open-circuit voltages can be expected with *p*-type compared with *n*-type absorbers.[17] The absorber thickness of ≈2.6 μm is much smaller than for the LPC absorber (6 μm), which may have caused worse light capturing and the lower measured short-circuit current density. We can thus assign the parameters achieved with our current CSS-SLG test cell to a not yet-optimized processing rather than to the material properties of the CSS mc-Si, which will be considered for the next investigations.

The PV parameters of these first representative solar cells on CSS-mc-Si on SLG are far away from the today's level of commercial crystalline silicon wafer material. One possible reason is that the bulk pristine CSS mc-Si material is processed without any further treatments such as hydrogen passivation. An alumina/aluminum composite layer at the interface between mc-Si and SLG together with a p^+/p junction working as the back surface field (BSF) has to take the function of back-side passivation, for which, however, we expect good quality since they are formed in the CSS process. A more severe issue is the surface-finishing step prior to HIT-emitter deposition, by which the active absorber layer was thinned to 2.6 μm (from ≈10 μm of pristine mc-Si). Thus, light capture and photocurrent density is strongly reduced. Furthermore, doping concentration in the residual layer is at least two orders of magnitude higher than in the removed silicon.[10] Therefore, bulk minority carrier lifetime is dominated by Auger recombination and probably drastically reduced with respect to 0.5 – 3 μs measured with the low-doped pristine CSS-mc-Si.

Table 1. Measured PV parameters of heterojunction-type solar cells on CSS-mc-Si, that is, open circuit voltage (V_{OC}), short-circuit current density (J_{SC}), fill factor (FF), conversion efficiency (Eff.), specific shunt (ρ_{sh}) and series resistivity (ρ_s), breakdown voltage (V_b), and active area.

No.	V_{oc} [mV]	J_{sc} [mA cm^{-2}]	FF [%]	Eff.[%]	R_{sh} [Ω cm^2]	R_s [Ω cm^2]	V_b [V]	Area [mm^2]
A	63	2.92	25.0	0.05	22	20	−0.1	3.61
B	343	7.00	49.4	1.18	408	13	−0.2	3.70
C	426	7.32	52.3	1.63	964	14	−0.4	3.69

 © 2024 The Author(s). Advanced Materials Interfaces published by Wiley-VCH GmbH
RIGHTSLINK

ADVANCED MATERIALS INTERFACES Open Access
www.advmatinterfaces.de

Correspondingly, a large saturation dark current density can be expected.

Trap-assisted recombination at the interface region of the emitter and absorber is another issue limiting the open circuit voltage and power conversion efficiency. Trap states in the absorber are analyzed using the measured current-density-versus-voltage characteristics of solar cell C (see Figure 4 and Table 1), which is shown in double-logarithmic representation in Figure S8 (Supporting Information). Here, we observe different linear regions, denoted by the Ohmic region at low bias voltage and trap-field-limit (TFL) region at intermediate bias voltages. At high bias voltages, beyond the scope of discussion, lies the space-charge-limiting-current region, which is not depicted here. The transition between Ohmic and TFL regions is given by a voltage V_{TFL} ($\approx$ 0.2 V), from which the trap-state density of the absorber can be calculated:[1]

$$N_{\mathrm{trap}} = \frac{2\varepsilon\varepsilon_0 V_{\mathrm{TFL}}}{q t_{\mathrm{ab}}^2} \tag{2}$$

with the relative dielectric constant of silicon (= 11.7), the dielectric constant of vacuum ε_0, the elementary charge q, and the absorber thickness t_{ab} (= 2.6 µm). We obtain $N_{\mathrm{trap}} = 3.8 \times 10^{13}$ cm^{-3}, which corresponds to the order of magnitude reported for *n*-type absorbers of mc-Si on glass by LPC.[18] HIT-emitter solar cell on these LPC absorbers showed an open-circuit voltage of 630 mV and an efficiency of 11.8%. Two orders of magnitude larger trap densities of 2.98 to 3.81 × 10^{15} cm^{-3} were observed with I-doped (*n*-type) Sb_2Se_3 absorbers on SLG.[1] A quasi-homojunction solar cell yielded an open-circuit voltage of 329 mV and an efficiency of 2.64% with an Sb_2Se_3 absorber containing acceptor-type antimony-vacancy defects of N_{trap} = 1.3 × 10^{13} cm^{-3}.[19] Technology Computer-Aided Design simulations with multi-/polycrystalline-Si solar cells showed that interface and grain-boundary trap densities in the range of 10^{13} cm^{-3} can cause efficiencies below 3 – 4%,[20] which is in agreement with our results. For further evaluation of the CSS solar cells, determination of external quantum efficiency and integrated short circuit current density J_{sc} will be required.[18,19]

It has been demonstrated that high-quality mc-Si thin films can be derived from SiO_2-containing SLG at low temperatures using CSS. These mc-Si thin films exhibit moderate acceptor concentrations, large grains, and a relatively high minority carrier lifetime, and these properties render such mc-Si thin films highly interesting in PV applications to lower the cost. The first batches of solar cells show very promising perspectives. However, there is still much work to be done in optimization of the quality of the mc-Si thin films as absorbers, for example, by further reducing the impurity level, increasing the grain size, passivating of the remaining crystal defects,[8,21] including light trapping micro- and nanostructures[22–24] to enhance the light absorption. In addition, a selective etching procedure should be optimized/developed, so that the local defective regions can be selectively removed without loss of active mc-Si materials. Furthermore, absorber thickness, emitter (a-Si:H or alternative)[25–27] and TCO contact[28] have to be optimized in order to improve the performance of solar cells with HIT emitter.

3. Conclusion

Multicrystalline silicon (mc-Si) thin films (≈10 µm) prepared on low-cost soda-lime glass by crystalline silicon synthesis (CSS) show large lateral grain sizes in the millimeter range, moderate doped *p*-type conductivity with an average Al acceptor concentration between 4.9 × 10^{16} and 1.2 × 10^{17} cm^{-3} in the bulk, and a minority carrier lifetime of 0.5 – 3 µs, which are essential for PV applications. First proof-of-concept solar cells with homojunction and heterojunction with intrinsic thin layer (HIT) emitters were prepared on the mc-Si thin films. A HIT solar cell with an open-circuit voltage of V_{OC} = 426 mV, a short-circuit current density of J_{SC} = 7.29 mA cm^{-2}, a fill factor of FF = 52.3% and a power conversion efficiency of η = 1.63% has been reached with an absorber thickness of ≈2.6 µm.

In future work, numerous steps are to be included in an optimized fabrication process as: 1) reducing the loss of active mc-Si materials by shorter surface etching (a much thinner damaged layer is expected using selective fs-laser ablation instead of diamond-paste polishing) of the thin chemically inert top layer, 2) reducing the recombination loss in CSS-mc-Si via hydrogen passivation of residual crystal defects and 3) by removing residual metal impurities from the silicon surface, 4) reducing optical loss by including light-trapping structures at the surface of the CSS-mc-Si, 5) optimizing the a-Si:H plasma-enhanced chemical vapor deposition of *p*-type mc-Si thin films (most HIT solar cells use *n*-type wafers), and 6) improving the transparent conducting oxide with respect to transparency, conductivity, and work function.

4. Experimental Section

As substrate for solar cells on multicrystalline (mc) silicon iron-poor SLG was used "Pilkington Optiwhite" (Pilkington Group Ltd, St. Helens, UK), which is a standard low-cost float glass. It is composed of 72.6% SiO_2, 13% Na_2O, 8.8% CaO, 4.3% MgO, 0.6% Al_2O_3, 0.02% SO_3 and 0.02% Fe_2O_3. The low concentration of iron oxide is confirmed by the lack of an otherwise appearing greenish shimmer caused by fluorescence under UV illumination. A mc-silicon layer is generated from the SLG using a layer of aluminum pressed onto it at 0.05-0.3 MPa and a temperature of 600 – 650 °C (well below the tensile fracture stress and softening point of the SLG) in normal ambient air using the so-called crystalline silicon synthesis (CSS) process.[9,10] The SLG has a Young's modulus and a linear thermal expansion coefficient of E = 72 MPa K^{-1} and α = 8.3 ppm K^{-1}.

A thin layer (20 to 50 nm) generated inherently at the surface of CSS mc-Si was analyzed using cross-sectional field-effect scanning electron microscopy (FE-SEM, 2 kV, 0.1 nA). Before, layers of Pt, C, and Au were deposited on the wafer for preparing the cross-section using a focused ion beam (FIB, Ga^+, 30 kV, 1.2 nA) combined with the FE-SEM for in-operando measurements (Helios 5 FX DualBeam, Thermo Scientific).

The element composition of the thin layer was determined under vertical incidence by XPS using a Kratos AXIS Supra XPS (Kratos Analytical Ltd., Manchester, United Kingdom) with a monochromatic Al-K_α source (1486.69 eV) at a chamber pressure of 2.3 × 10^{-7} Pa. The high-resolution spectra of the O 1s, Si 2p, and Al 2p states displayed in Figure S2 (Supporting Information) were obtained using a step size of 0.1 eV and a pass energy of 20 eV. Analysis of the XPS data was done using CasaXPS, version 2.3.25.

For structural analysis of the thin layer, X-ray diffraction was done on a Bruker D8 Advance Bragg-Brentano diffractometer operating with Cu-Kα radiation and using a 1D silicon strip detector (LynxEye). Here, a snippet of CSS-mc-Si (Al residues not etched in AL 80) cut from its SLG substrate

© 2024 The Author(s). Advanced Materials Interfaces published by Wiley-VCH GmbH
RIGHTSLINK
21967350, 2024, 28, Downloaded from https://onlinelibrary.wiley.com/doi/10.1002/admi.202400170 by Fak-Martin Luther Universitats, Wiley Online Library on [05/11/2024]. See the Terms and Conditions (https://onlinelibrary.wiley.com/terms-and-conditions) on Wiley Online Library for rules of use; OA articles are governed by the applicable Creative Commons License

was fixed on adhesive tape and investigated from bottom- and top-side of the mc-Si.

The layer was found to be chemically resistant to wet etching in common alkalis and acids (sodium hydroxide (NaOH), HF, phosphoric acid (H_3PO_4)) and inductive-coupled plasma (ICP) dry etching (RIE, using SF_6, ICP-RIE plasma etcher SI 500, SENTECH, Germany or PlasmaPro 100 RIE, Oxford Instruments, UK). It could be removed only physically with fs-pulse laser ablation (140 mW – 3 W, Yb-based femtosecond laser source, Spirit-1040, Spectra-Physics, almost selective over silicon) or by polishing with diamond paste (0.25 µm, Struers GmbH, Hannover, Germany) for 90 s. Damage to the mc-Si had to be removed afterward using etching in anisotropic KOH (25 wt%, 55 °C, 90 s) or in isotropic perchloric-acid-based solution (nitric acid (HNO_3), 65 wt% : hydrofluoric acid (HF), 40 wt% : acetic acid (CH_3COOH), 100 wt% : perchloric acid ($HClO_4$), 60 wt% = 75 : 7:10 : 8, by volume) solutions.

Al concentration profiles in mc-Si were measured using SIMS in a Hiden Analytical SIMS Workstation operated with 5 keV O^+ ions for sputtering on an area of ≈50 × 50 µm2. The sputtered ions were analyzed from an area of 5 × 5 μm^2 within the developing crater, with uncertainties in concentration and depth amounting of less than ± 10% and ± 50 nm, respectively. A CSS mc-Si sample with an Al concentration of 3 – 5 × 10^{18} cm^{-3} was used as reference.[10]

Stress in mc-Si on SLG was determined using Raman spectroscopy in a micro-PL/Raman spectroscopy system equipped with an Olympus BH2 BHSM microscope. The microscope was coupled to a Jobin Yvon U1000 double monochromator with 1000 mm focal length and 1800 gr mm^{-1} gratings and a Horiba Synapse FIVS CCD detector. A frequency-doubled diode-pumped solid state laser system "Genesis MX532-1000 STM" with a wavelength of $\lambda = 532$ nm was used as an excitation source. The incident excitation energy was kept low (160 µW, 30 s) to avoid excessive photo-generation of free charge carriers. Using an objective (magnification: 100×, NA = 0.9) a diffraction-limited beam-spot diameter of 0.7 µm was realized corresponding to the diameter of the diffraction disc (1.22 λ NA^{-1}).

Activation of the implanted phosphorus profiles in the emitter of homojunction diodes was investigated using ECV profiling (CVP21 profiler, WEP, Furtwangen, Germany). ECV was performed employing an ammonium bifluoride solution (NH_4HF_2, 0.57 wt%) as electrolyte and a contact to the silicon defined by a sealing ring of 1 mm in diameter. The depth scale is defined by an anodic dissolution reaction.[29] For the measured concentrations an uncertainty of 10% to 20% was assumed.[30] The dimensions and surface roughness of the generated crater were controlled using CLSM (LEXT OLS5100, Olympus).

HIT emitters were fabricated on CSS mc-Si as depicted in Figure 1. The CSS process is started with an Al layer deposited on SLG (Figure 1a). During CSS a mc-silicon layer is formed with a composite layer of alumina and unreacted Al underneath (Figure 1b). A thin chemically inert alumina/aluminosilicate layer at the surface of the mc-Si (cf. Figure S1, Supporting Information) is removed by polishing for 90 s with diamond paste (Struers GmbH, Hannover, Germany, 0.25 µm). Afterwards, the wafer is etched in KOH (25 wt% KOH, 55 °C, 90 s) resulting in a removal of ≈1 µm of mc-Si.

To fabricate the HIT-emitter-type solar cells, the CSS mc-Si thin film was first dipped in a buffered HF solution (2%) for 2 min to remove the intrinsic SiO_x thin layer. The following step of etching in an isotropic perchloric-acid-based etching solution containing HNO_3 (65 wt%) : HF (40 wt%) : CH_3COOH (100 wt%) : $HClO_4$ (60 wt%) = 75 : 7:10 : 8 (in volume). The samples B and C were etched in this solution for 4 and 20 s, resulting in a dissolved layer at the top mc-Si of 1 and 5 µm, respectively. This step intends to remove remaining polishing damage layer and to reduce surface roughness (etching rate determined on a monocrystalline silicon wafer is ≈15 µm min^{-1}.). The sample was rinsed thoroughly with deionized water afterward, followed by a cleaning procedure in Piranha solution (sulfuric acid (H_2SO_4: 98 wt%) : hydrogen peroxide (H_2O_2: 30 wt%) = 1 : 1 in vol. : vol.) solution for 15 min to remove contaminations. A HF (2%) dip for 2 min was performed to remove the SiO_x grown during the Piranha-solution cleaning and the sample was quickly transferred into the PECVD chamber after thoroughly rinsing with deionized water. Layers of 3-nm-thick intrinsic and ≈15-nm-thick highly n^+-type a-Si:H were deposited on the mc-Si and served as the emitter of the HIT solar cells. The process temperature was 225 °C (Figure 1c). The TCO consisted of 1 nm Al_2O_3 followed by 200 nm AZO deposited both by ALD at 225 °C. The 1-nm Al_2O_3 served as ultrathin tunneling passivation contact (Figure 1d).[28]

Mesa cells were prepared by locally deposited photoresist heated in a furnace at 80 °C for 30 min (Figure 1e). The sample is then etched in the above-mentioned perchloric-acid-based solution for 40 s to remove the AZO layer, the thin Al_2O_3, and the a-Si:H emitter outside the areas protected by the photoresist (Figure 1f). After a copious rinsing with deionized water, the photoresist was removed by soaking with acetone, so that the active areas of the solar cell were exposed. The rear contact was prepared by scratching of InGa alloy on the mc-Si base layer around the mesa cells, which forms an Ohmic contact on the substrate. Surface topography and roughness of the completed device structure were controlled using CLSM (LEXT OLS5100, Olympus).

Current-versus-voltage curves were taken with the solar cells using a Keithley 236 Source Measure Unit in the dark and in a solar simulator under AM 1.5 G (100 $mWcm^{-2}$) illumination. The current was divided by the active-cell area, which was determined by a microscope for each device, yielding current density. The results of the best cells from each run are shown in Figure 4 and Table 1.

Supporting Information

Supporting Information is available from the Wiley Online Library or from the author.

Acknowledgements

This work was funded by the Deutsche Bundesstiftung Umwelt (DBU) in three projects (Az.: 32945/01, /02, /03) as well as by the German Federal Ministry for Economic Affairs and Energy (BMWi, 03THWNI009), the Lower Saxony Ministry of Science and Culture and the Institute for Semiconductor Technology of the Technische Universität Braunschweig in a project through the directive of WIPANO (Wissens- und Technologietransfer durch Patente und Normen). This research was further funded by the Thuringian Ministry of Economy, Science and Digital Society within the Infralith project (2021 FGI 0020) co-financed by the European Union within the European Regional Development Fund (ERDF).

Open access funding enabled and organized by Projekt DEAL.

Conflict of interest

The authors declare no conflict of interest.

Data Availability Statement

The data that support the findings of this study are available from the corresponding author upon reasonable request.

Keywords

aluminothermic reaction, heterojunction-emitter solar cell, multicrystalline silicon, soda-lime glass, thin film

Received: February 23, 2024
Revised: August 7, 2024
Published online: September 2, 2024

© 2024 The Author(s). Advanced Materials Interfaces published by Wiley-VCH GmbH

RIGHTSLINK

21967350, 2024, 28, Downloaded from https://onlinelibrary.wiley.com/doi/10.1002/admi.202400170 by Fak-Martin Luther Universitats, Wiley Online Library on [05/11/2024]. See the Terms and Conditions (https://onlinelibrary.wiley.com/terms-and-conditions) on Wiley Online Library for rules of use; OA articles are governed by the applicable Creative Commons License

[1] D. Ren, S. Chen, M. Cathelinaud, G. Liang, H. Ma, X. Zhang, *ACS Appl. Mater. Interfaces* **2020**, *12*, 30572.
[2] P. Fan, J. Lin, J. Hu, Z. Yu, Y. Zhao, S. Chen, Z. Zheng, J. Luo, G. Liang, Z. Su, *Adv. Funct. Mater.* **2022**, *32*, 2207470.
[3] M. L. Hsieh, A. Kaiser, S. Bhattacharya, S. John, S. Y. Lin, *Sci. Rep.* **2020**, *10*, 11857.
[4] J. Plentz, T. Schmidt, A. Gawlik, J. Bergmann, G. Andrä, D. Hauschild, V. Lissotschenko, *Phys. status solidi* **2017**, *214*, 1600882.
[5] P. Sonntag, M. Bokalič, N. Preissler, D. Amkreutz, B. Rech, M. Topič, *Sol. Energy Mater. Sol. Cells* **2018**, *181*, 2.
[6] S. Garud, C. T. Trinh, D. Abou-Ras, B. Stannowski, R. Schlatmann, B. Rech, D. Amkreutz, *Sol. RRL* **2020**, *4*, 2000058
[7] P. Sonntag, N. Preissler, M. Bokalič, M. Trahms, J. Haschke, R. Schlatmann, M. Topič, B. Rech, D. Amkreutz, *Sci. Rep.* **2017**, *7*, 873.
[8] S. Kühnapfel, S. Severin, N. Kersten, P. Harten, B. Stegemann, S. Gall, *Sol. Energy Mater. Sol. Cells* **2019**, *203*, 110168.
[9] E. Peiner, A. Waag, G. Palm, I. Schall, H. Schall, *European Patent EP 3513425B102016117182A1*, **2022**.
[10] I. Schall, S. G. Ebbinghaus, C. Strelow, E. Peiner, *Adv. Mater. Interfaces* **2023**, *10*, 2300681.
[11] T. Antesberger, T. A. Wassner, M. Kashani, M. Scholz, R. Lechner, S. Matich, M. Stutzmann, *J. Appl. Phys.* **2012**, *112*, 123509.
[12] M. Rauer, C. Schmiga, M. Glatthaar, S. W. Glunz, *Sol. Energy Mater. Sol. Cells* **2018**,*176*, 295.
[13] J. Dziewior, W. Schmid, *Appl. Phys. Lett.* **1977**, *31*, 346.
[14] A. Richter, S. W. Glunz, F. Werner, J. Schmidt, A. Cuevas, *Phys. Rev. B* **2012**, *86*, 165202.
[15] M. Vetter, A. Gawlik, J. Plentz, G. Andrä, *Energy Procedia* **2016**, *92*, 248.
[16] D. Ren, B. Fu, Z. Li, B. Zhu, C. Li, J. Ji, S. Chen, H. Ma, X. Zhang, *Vacuum* **2023**, *215*, 112393.
[17] J. Haschke, D. Amkreutz, T. Frijnts, S. Kühnapfel, T. Hänel, B. Rech, *IEEE J. Photovoltaics* **2015**, *5*, 1001.
[18] D. Amkreutz, W. D. Barker, S. Kühnapfel, P. Sonntag, O. Gabriel, S. Gall, U. Bloeck, J. Schmidt, J. Haschke, B. Rech, *IEEE J. Photovoltaics* **2015**, *5*, 1757.
[19] D. Ren, C. Li, Z. Li, B. Zhu, B. Fu, J. Ji, S. Chen, G. Liang, H. Ma, X. Zhang, *J. Alloys Compd.* **2023**, *960*, 170753.
[20] M. Imam, T. Ahmed, S. S. A. Askari, *Arabian J. Sci. Eng.* **2024**, *49*, 995.
[21] G. Jia, G. Andrä, A. Gawlik, S. Schönherr, J. Plentz, B. Eisenhawer, T. Pliewischkies, A. Dellith, F. Falk, *Sol. Energy Mater. Sol. Cells* **2014**, *126*, 62.
[22] G. Jia, M. Steglich, I. Sill, F. Falk, *Sol. Energy Mater. Sol. Cells* **2012**, *96*, 226.
[23] M. Vetter, G. Jia, A. Sanei, A. Gawlik, J. Plentz, G. Andrä, *Phys. Status Solidi A* **2017**, *214*, 1600859.
[24] G. Jia, A. Gawlik, J. Plentz, G. Andrä, *Sol. Energy Mater. Sol. Cells* **2017**, *167*, 102.
[25] A. Gawlik, J. Plentz, I. Höger, G. Andrä, T. Schmidt, U. Brückner, F. Falk, *Phys. Status Solidi A* **2015**, *212*, 162.
[26] A. Gawlik, I. Höger, J. Bergmann, J. Plentz, T. Schmidt, F. Falk, G. Andrä, *Phys. Status Solidi RRL* **2015**, *9*, 397.
[27] M. Junghanns, J. Plentz, G. Andrä, A. Gawlik, I. Höger, F. Falk, *Appl. Phys. Lett.* **2015**, *106*, 083904.
[28] G. Jia, B. Eisenhawer, J. Dellith, F. Falk, A. Thøgersen, A. Ulyashin, *J. Phys. Chem. C* **2013**, *117*, 1091.
[29] E. Peiner, A. Schlachetzki, *J. Electrochem. Soc.* **1992**, *139*, 552.
[30] E. Peiner, A. Schlachetzki, D. Krüger, *J. Electrochem. Soc.* **1995**, *142*, 576.

© 2024 The Author(s). Advanced Materials Interfaces published by Wiley-VCH GmbH
RIGHTSLINK Copyright Clearance Center
21967350, 2024, 28, Downloaded from https://onlinelibrary.wiley.com/doi/10.1002/admi.202400170 by Fak-Martin Luther Universitats, Wiley Online Library on [05/11/2024]. See the Terms and Conditions (https://onlinelibrary.wiley.com/terms-and-conditions) on Wiley Online Library for rules of use; OA articles are governed by the applicable Creative Commons License